Available online at www.sciencedirect.com

ScienceDirect

Mendeleev Commun., 2022, **32**, 759–762

Mendeleev Communications

Coordination polymers derived from magnesium and barium complexes of redox-active ligands

Natalia L. Bazyakina,[a] Valentin M. Makarov,[a] Mikhail V. Moskalev,[a] Evgeny V. Baranov,[a] Artem S. Bogomyakov,[b] Victor I. Ovcharenko[b] and Igor L. Fedushkin*[a]

[a] *G. A. Razuvaev Institute of Organometallic Chemistry, Russian Academy of Sciences, 603137 Nizhny Novgorod, Russian Federation. E-mail: igorfed@iomc.ras.ru*

[b] *International Tomography Center, Siberian Branch of the Russian Academy of Sciences, 630090 Novosibirsk, Russian Federation*

DOI: 10.1016/j.mencom.2022.11.017

The reactions of monomeric complexes [(dpp-bian)M(THF)$_n$] (M = Mg, n = 3; M = Ba, n = 5; dpp-bian = 1,2-bis[(2,6-diisopropylphenyl)imino]acenaphthene) with 4,4′-bipyridine (4,4′-bipy) in THF proceed with electron transfer from dpp-bian^{2-} to 4,4′-bipy^0 to afford 1D coordination polymers [(dpp-bian)M(4,4′-bipy)(THF)$_n$]$_m$ (M = Mg, n = 1; M = Ba, n = 2) that contain simultaneously radical anion ligands dpp-bian$^-$ and 4,4′-bipy. Addition of DME to coordination polymer [(dpp-bian)Mg(4,4′-bipy)(THF)$_n$]$_m$ results in fragmentation of polymeric chains to give dinuclear magnesium species [{(dpp-bian)Mg(DME)}$_2$(4,4′-bipy)]. Barium analogue [{(dpp-bian)Ba(DME)$_2$}$_2$(4,4′-bipy)] has been prepared by reacting of complex [(dpp-bian)Ba(DME)$_{2.5}$] with 4,4′-bipy in DME.

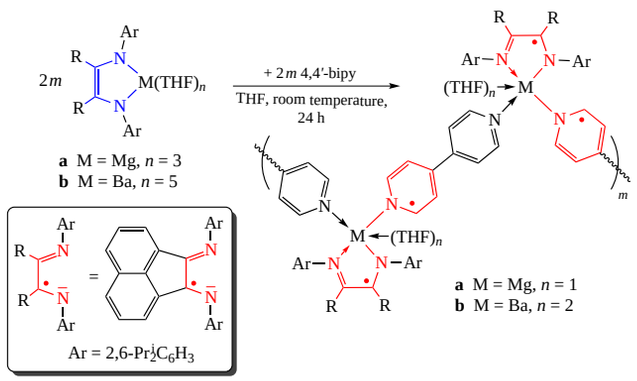

Keywords: magnesium complexes, barium complexes, redox-active ligands, metal–organic coordination polymers, X-ray diffraction.

Metal–organic coordination polymers (MOCPs) represent crystalline materials with unique properties.[1–4] From thousands of MOCPs prepared annually a few reveal redox properties due to the metal,[5] terminal organic ligand or organic linker,[6,7] or guest molecules.[8,9] Redox-active MOCPs provide for the possibility of switching their spectral, magnetic, electronic and other properties by changing the redox states of the building blocks.[10–15] On the other hand, redox process at each redox-active site can lead to a change in molecular geometry of the polymeric chains and, in its turn, to an alteration of a voids volume.[16] This will probably affect the guest molecules and lead to either their liberation or activation towards chemical transformations. Recently we have reported formation of calcium and strontium coordination polymers by reacting mononuclear [(dpp-bian)M(THF)$_4$] (M = Ca or Sr; dpp-bian = dianion of 1,2-bis[(2,6-diisopropylphenyl)imino]acenaphthene) with 4,4′-bipyridine (4,4′-bipy) in THF or THF/benzene. Coordination of 4,4′-bipy to metal centres in [(dpp-bian)M(THF)$_4$] (M = Ca or Sr) is accompanied with transfer of an electron from dpp-bian^{2-} to 4,4′-bipy^0 and formation of 1D metal–organic coordination polymers, [(dpp-bian)M(4,4′-bipy)(THF)$_2$]$_m$ (M = Ca or Sr).[17] Interestingly, on dissolution of two latter products in THF a back electron transfer from 4,4′-bipy$^-$ to dpp-bian$^-$ takes place. This facile interchange between redox states (dpp-bian^{2-} and dpp-bian$^-$) is distinctive of the dpp-bian[18] and may provide for preparation of bistable coordination polymers. Considering the advantages of the simultaneous presence of dpp-bian and 4,4′-bipy in MOCPs derived from group 2 metals we turned to two other representatives of the 2nd group, namely, Mg and Ba. Here we report preparation and characterization of their coordination polymers that represent lighter and heavier analogues of the Ca and Sr derivatives. Also we report solvent-induced reversible fragmentation of these MOCPs to dinuclear species.

Addition of one equivalent of 4,4′-bipy to solutions of [(dpp-bian)M(THF)$_n$] (**1a** M = Mg, n = 3; **1b** M = Ba, n = 5) in

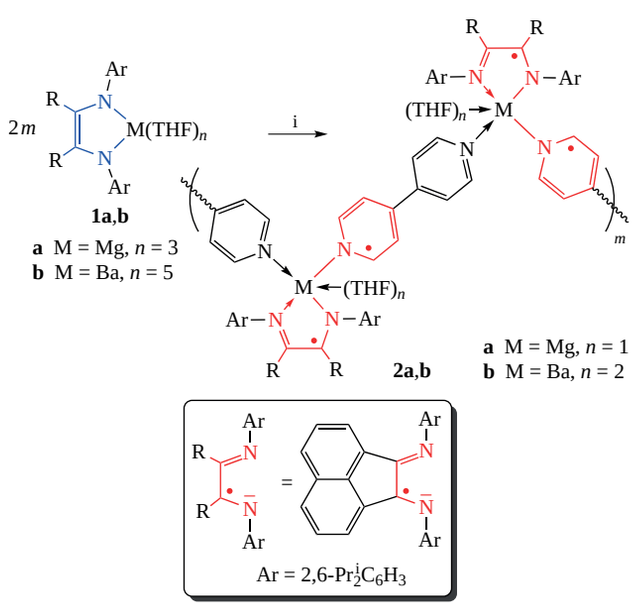

Scheme 1 *Reagents and conditions*: i, 4,4′-bipy (2 equiv.), THF, room temperature, 24 h.

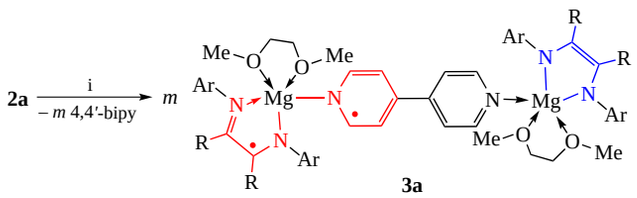

Scheme 2 *Reagents and conditions*: i, DME, room temperature.

THF causes an immediate colour change of the reaction mixtures from dark green (**1a**) and brown (**1b**) to deep blue and formation of 1D coordination polymers $[(dpp\text{-}bian)M(4,4'\text{-}bipy)(THF)_n]_m$ (**2a** M = Mg, n = 1; **2b** M = Ba, n = 2) (Scheme 1).

A low quality of crystals of **2a** and **2b** prevented an assessment of the bond lengths and angles in compounds **2a** and **2b** by the single crystal X-ray analysis. However, it has allowed establishment of the atom connectivity in both products. In attempt to prepare crystals suitable for the X-ray analysis, compound **2a** was recrystallized from DME. Unexpectedly, monomeric dinuclear complex $[(dpp\text{-}bian)^{-}Mg(DME)(4,4'\text{-}bipy)^{-}(dpp\text{-}bian)^{2-}Mg(DME)]$ **3a** was isolated (Scheme 2).

An attempted crystallization of compound **2b** from DME failed. Moreover, barium analogue of the magnesium complex **3a**, *viz*. $[(dpp\text{-}bian)^{2-}Ba(DME)_2(4,4'\text{-}bipy)^{0}(dpp\text{-}bian)^{2-}Ba(DME)_2]$ **3b** was also not formed. However, complex **3b**, was prepared by the reaction of **1b**·DME with 0.5 equiv. of 4,4′-bipy in DME (Scheme 3).

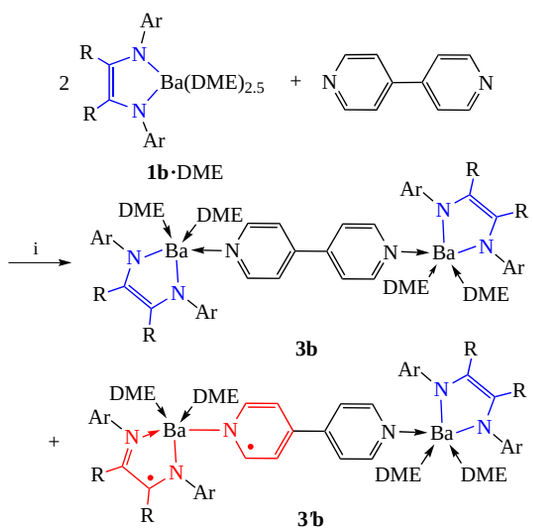

Scheme 3 *Reagents and conditions*: i, DME, room temperature.

Air oxygen and moisture decompose compounds **2a**,**b** to release molecules of THF, dpp-bian and 4,4′-bipy as confirmed by the ^{1}H NMR spectroscopy. The ^{1}H NMR spectra of the mixtures obtained in the course of destruction of compounds **2a**,**b** indicate the presence of free dpp-bian and 4,4′-bipy in a molar ratio 1 to 1 (see Online Supplementary Materials, Figures S1 and S2, respectively).

Molecular structures of **2a**, **2b**, **3a** and **3b** have been determined by the single crystal X-ray analysis (Figures 1, 2 and S1, S2 of Online Supplementary Materials).[†] The structural motif

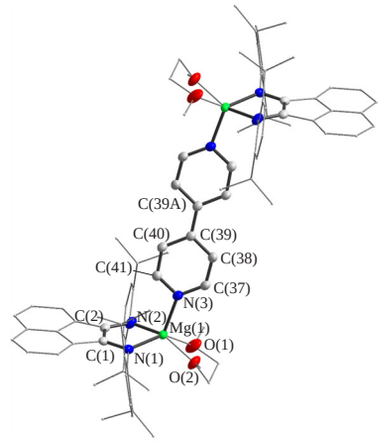

Figure 1 Molecular structure of **3a**. Thermal ellipsoids are drawn at 50% probability level. Hydrogen atoms are omitted. Selected bond lengths (Å): Mg(1)–N(1) 2.0705(16), Mg(1)–N(2) 2.0864(16), Mg(1)–N(3) 2.0755(16), C(1)–C(2) 1.413(2), N(1)–C(1) 1.360(2), N(2)–C(2) 1.357(2), Mg(1)–O(1) 2.1240(16), Mg(1)–O(2) 2.1373(15), N(3)–C(37) 1.360(2), N(3)–C(41) 1.367(2), C(37)–C(38) 1.367(2), C(38)–C(39) 1.430(2), C(39)–C(40) 1.424(2), C(40)–C(41) 1.367(2), C(39)–C(39A) 1.426(3).

in **2a**,**b** is very similar to that of Ca and Sr analogues reported just recently.[17] Thus, compounds **2a**,**b** consist of infinite 1D zigzag chains that are built of the M^{2+} ions and radical anionic 4,4′-bipy linkers. Terminal dpp-bian ligand also serves as radical anion. In analogy to the Ca and Sr derivatives, the coordination polymers **2a**,**b** consist of the voids that are filled with solvent molecules: two and a half THF molecules in **2a** and four THF molecules in **2b**. The barium atom in **2b** coordinates two THF molecules, but in compound **2a** a smaller ionic radius of magnesium allows coordination of only one THF molecule. Different coordination numbers of Mg and Ba atoms in **2a** and **2b** cause different mutual arrangements of the ligands. In coordination polymer **2a** the dihedral angles between the plane of the dpp-bian (defined with Mg and two N atoms) and the planes of two 4,4′-bipy (defined N and two adjacent C atoms) are 55 and 90° (Figure S3). The dihedral angle between the planes of two 4,4′-bipy ligands is 58°. In contrast, for derivative **2b** the planes of dpp-bian and 4,4′-bipy are practically coincide (Figure S4). Crystals of **3a** and **3b** consist of discrete dinuclear molecules (see Figures 1 and 2, respectively).

[†] *Crystallographic data for* **3a**. Crystals of $C_{103.6}H_{142}Mg_2N_6O_{10.8}$ (M = 1692.91) are monoclinic, space group $P2(1)/c$, at 100 K, a = 17.7424(11), b = 17.2264(10) and c = 15.7100(10) Å, α = 90°, β = 92.987(2)°, γ = 90°, V = 4795.0(5) Å^3, Z = 2, d_{calc} = 0.960 g cm^{-3}, crystal size 0.66×0.54×0.29 mm, μ(MoKα) = 0.070 mm^{-1}, F(000) = 1492. 59461 reflections were measured and 11537 independent reflections (R_{int} = 0.0473) were used in a further refinement. The refinement converged to wR_2 = 0.1781 and GOF = 1.032 for all independent reflections [R_1 = 0.0661 was calculated against F for 9094 observed reflections with $I > 2\sigma(I)$].

Crystallographic data for **3b**. Crystals of $C_{98}H_{128}Ba_2N_6O_8$ (M = 1792.74) are monoclinic, space group $P2(1)/n$ at 100 K, a = 11.3305(5), b = 18.6453(8) and c = 21.2072(10) Å, α = 90°, β = 91.0977(16)°, γ = 90°, V = 4480.2(3) Å^3, Z = 2, d_{calc} = 1.329 g cm^{-3}, μ(MoKα) = 0.932 mm^{-1}, F(000) = 1868. 73031 reflections were measured and 13681 independent reflections (R_{int} = 0.0474) were used in a further refinement. The refinement converged to wR_2 = 0.0694 and GOF = 1.028 for all independent reflections [R_1 = 0.0294 was calculated against F for 12312 observed reflections with $I > 2\sigma(I)$].

The X-ray diffraction data for **2a**, **2b**, **3a** and **3b** were collected with Rigaku OD SuperNova (**2a**, CuKα-radiation, ω-scans technique, λ = 1.54184 Å) and Bruker D8 Quest (**2b**, **3a** and **3b**, MoKα-radiation, ω-scans technique, λ = 0.71073 Å). The intensity data were integrated by SAINT[28] program. SADABS[29] was used to perform absorption corrections. The structures were solved by dual method using SHELXT[30] and refined on F^2_{hkl} using SHELXTL package.[31,32] All non-hydrogen atoms were refined anisotropically. All hydrogen atoms were placed in calculated positions and were refined in the riding model [$U_{iso}(H)$ = 1.5 $U_{eq}(C)$ for CH_3-groups and $U_{iso}(H)$ = 1.2 $U_{eq}(C)$ for other groups]. Disordered DME molecules in **3a** were squeezed using Platon.[33]

CCDC 2116965 (**3a**) and 2116966 (**3b**) contain the supplementary crystallographic data for this paper. These data can be obtained free of charge from The Cambridge Crystallographic Data Centre *via* http://www.ccdc.cam.ac.uk.

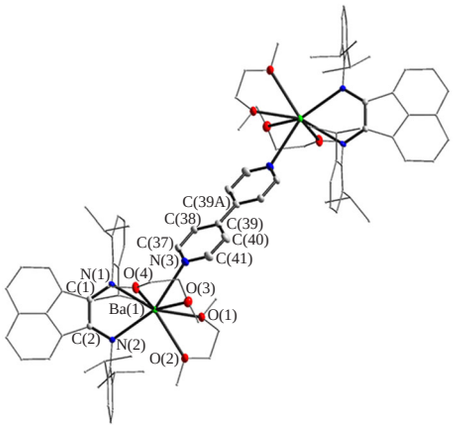

Figure 2 Molecular structure of **3b**. Thermal ellipsoids are drawn at 50% probability level. Hydrogen atoms are omitted. Selected bond lengths (Å): Ba(1)–N(1) 2.6970(18), Ba(1)–N(2) 2.6640(18), Ba(1)–N(3) 2.920(2), C(1)–C(2) 1.411(3), N(1)–C(1) 1.378(3), N(2)–C(2) 1.370(3), Ba(1)–O(1) 2.9228(15), Ba(1)–O(2) 2.9131(18), Ba(1)–O(3) 2.9560(16), Ba(1)–O(4) 2.7335(15), N(3)–C(37) 1.339(3), N(3)–C(41) 1.340(3), C(37)–C(38) 1.387(3), C(38)–C(39) 1.386(3), C(39)–C(40) 1.397(4), C(40)–C(41) 1.383(3), C(39)–C(39A) 1.482(4).

The crystallographic inversion centre in both compounds is located in the middle of C(39)–C(39A) bond of 4,4′-bipy. The magnesium atoms in **3a** are five-coordinate. The C(1)–N(1) and C(2)–N(2) bond lengths [1.360(2) and 1.357(2) Å, respectively] in dpp-bian in complex **3a** lie in between those values observed in dpp-bian radical anions and dianions. Thus, the C(1)–N(1) and C(2)–N(2) distances in dpp-bian radical-anions are close to 1.33 Å, as for instance in five-coordinate [(dpp-bian)MgSBu^s(DME)] [1.3296(13) and 1.3345(14) Å][19] and four-coordinate dinuclear [{(dpp-bian)Mg(THF)}$_2$(N_2Ph_2)] [1.337(3) and 1.339(3) Å].[20] On going from the radical anion to dianion the C(1)–N(1) and C(2)–N(2) bonds lengthen to 1.39 Å, as for example in [(dpp-bian)Mg(THF)$_3$][21] (*av*. 1.39 Å). Similarly, the Mg–N(1) and Mg–N(2) bond lengths in **3a** (*av*. 2.078 Å) are shorter than in [(dpp-bian)MgSBu^s(DME)] (*av*. 2.132 Å)[19] and [{(dpp-bian)Mg(THF)}$_2$(N_2Ph_2)] (*av*. 2.116 Å),[20] close to those in [(dpp-bian)Mg(THF)$_3$][21] (*av*. 2.075 Å) and longer than in [(dpp-bian)Mg(THF)$_2$][21] (*av*. 1.995 Å). The intermediary values of the C–N and Mg–N bond lengths in **3a** may indicate the simultaneous presence of dpp-bian radical anion and dianion, whose superposition results in the averaging of the C–N and Mg–N distances. The C–N bond lengths in 4,4′-bipy ligand in complex **3a** (*av*. 1.363 Å) are well compared with those values in 4,4′-bipy radical anions in [Na_2(4,4′-bipy)$_2$(en)$_2$]$_m$ and [Na(4,4′-bipy)(en)]$_m$ (*av*. 1.353 and 1.357 Å, respectively).[22] In compound **3b** (see Figure 2) the bond lengths C(1)–N(1) and C(2)–N(2) [1.378(3) and 1.370(3) Å, respectively] allow suggesting the dianionic state of dpp-bian ligands.[23] Indirect evidence for that might be the geometry of 4,4′-bipy ligand. If the latter serves as neutral, both dpp-bian ligands represent dianions. On going from neutral 4,4′-bipy to its radical anion and further to dianion the C–N distances lengthen. In complex **3b** the bond lengths N(3)–C(37) and N(3)–C(41) [1.339(3) and 1.340(3) Å, respectively] are shorter than in **3a** [1.360(2) and 1.367(2) Å] as well as in [Na_2(4,4′-bipy)$_2$(en)$_2$]$_m$ and [Na(4,4′-bipy)(en)]$_m$[22] [1.352(2)–1.360(2); 1.364(2)–1.371(2); 1.423(2)–1.430(2); 1.423(2)–1.424(3) Å] that contain the radical anion of 4,4′-bipy. Another evidence for a neutral state of 4,4′-bipy in **3b** is the value of the C(39)–C(39A) bond. This bond length is shortened on going from the neutral 4,4′-bipy (*av*. 1.482 Å) to its radical anion (*av*. 1.420 Å) and dianion [1.373(4) Å].[24] This is exactly case for **3a** and **3b** [–1.482(4) and 1.426(3) Å, respectively].

The TGA curves for compounds **2a** and **2b** are depicted in Figure S5 (see Online Supplementary Materials). For compound **2a** in the first stage (7%, 30–79 °C, max. rate at 42 °C) the sample releases solvent molecules, that corresponds to one THF molecule. The next stage (14%, 107–223 °C, max. rate at 167 °C) is associated with removal of two THF molecules. Compound **2b** loses weight gradually on heating to 250 °C due to the removal of the solvent molecules both coordinated and present in the lattice. A thermal destruction of the chains **2a** and **2b** takes place at 317 °C.

The temperature dependencies of the effective magnetic moment (μ_{eff}) of products **2a**,**b** are shown in Figure S6. At 300 K the μ_{eff} values are 2.45 and 2.44 μ_B for the complexes **2a** and **2b**, respectively, and are in good agreement with theoretical spin-only value of 2.45 μ_B for two non-interacting radicals. For the product **2a** the μ_{eff} value is nearly constant in the range 300–150 K, and below 150 K the μ_{eff} decreases down to 0.49 μ_B at 2 K. In contrast, for compound **2b** the μ_{eff} changes insignificantly in the temperature range 300–40 K and decreases only below 40 K to 1.78 μ_B at 2 K. The observed $\mu_{eff}(T)$ dependencies indicate the presence of quite strong antiferromagnetic exchange between radicals in compound **2a**, whereas antiferromagnetic coupling in **2b** is much weaker. The experimental data have been analyzed using a model for antiferromagnetically coupled chains. The best fit values of g factors and exchange coupling parameters are: $g = 2.054 \pm 0.002$, $J_1 = -0.90 \pm 0.03$ cm^{-1} and $J_2 = -7.02 \pm 0.06$ cm^{-1} for **2a** and $g = 1.980 \pm 0.001$, $J_1 = -1.06 \pm 0.09$ cm^{-1} and $J_2 = -0.53 \pm 0.04$ cm^{-1} for **2b**. The comparison of these data with those obtained for the analogues [(dpp-bian)Ca(4,4′-bipy)(THF)$_2$]$_m$ (0 and –4.6 cm^{-1}) and [(dpp-bian)Sr(4,4′-bipy)(THF)$_2$]$_m$ (–0.14 and –3.7 cm^{-1})[17] allows concluding that lessening of the energy of exchange interaction between spins of 4,4′-bipy and dpp-bian radical anions correlates with the increase of the metal ionic radii.

The presence of the radical anionic ligands in products **2a**, **2b** and **3a** deduced from structural and magnetic data (for **2a**,**b**) is further confirmed by ESR spectroscopy. The crystalline samples of **2a**, **2b** and **3a** reveal ESR signals, whose g values (g = 2.0042, 2.0040 and 2.0039) are indicative for the presence of unpaired electrons (Figure S7). According to the X-ray data, compound **3b** should be diamagnetic. However, in the solid state it also reveals ESR signal (g = 2.0031) probably due to admixture of electronic isomer **3′b** (see Scheme 3). The presence of the admixture of radical anionic species in **3b** is confirmed by the IR spectroscopy: a moderate intensity absorption at 1536 cm^{-1} (Figure S9) is typical for stretching vibrations of C–N bonds in the dpp-bian radical anion.[19] A dissolution of **2a**,**b** in THF is accompanied with the electron transfer from 4,4′-bipy back to dpp-bian and affords starting compounds **1a,b** together with free 4,4′-bipy. As expected, the solutions formed are ESR silent. Compounds **3a**,**b** reveal at 298 K in DME solution the ESR signals that exhibit hyper-fine structures (Figures S10, S11). Simulation of the signals using EasySpin[25] software revealed the best result for equimolar quantities of dpp-bian and 4,4′-bipy radical anions. Thus, the experimental spectra of **3a**,**b** represent superposition of the signals of dpp-bian and 4,4′-bipy. The presence of radical anion of 4,4′-bipy in DME solution of **3a** was confirmed by UV-VIS spectroscopy (maxima at 568 and 644 nm, Figure S12)[26], while in DME solution of **3b** it was not detected probably due to its low concentration. Compounds **2a**,**b** are poorly soluble in non-coordinating solvents. In contrast, they are readily soluble in THF to afford solutions that exhibit broad absorption bands with maxima at 850 nm (**2a** and **3a**) and 900 nm (**2b** and **3b**) thus signifying the formation of the starting **1a**,**b**. This process is triggered by interaction of the coordinating solvent molecules with the metal ions and accompanied with back electron transfer from the bridging 4,4′-bipy radical anion

to $[(dpp\text{-}bian)M]^+$ (M = Mg or Ba). Just recently such behavior has been observed on the related calcium and strontium complexes[17] as well as group 1 metal species derived from dpp-bian and 4,4′-bipy.[27]

In conclusion, we reported the completion of the synthesis and characterization of the Mg and Ba 1D coordination polymers, $[(dpp\text{-}bian)^{-}M(4,4'\text{-}bipy)^{-}(THF)_n]_m$ (**2a** M = Mg, n = 1; **2b** M = Ba, n = 2). In diluted THF solutions, substances **2a**,**b** undergo fragmentation to starting compounds. Also, in DME solution the fragmentation of **2a** takes place but brings about dimeric $[(dpp\text{-}bian)^{-}Mg(DME)(4,4'\text{-}bipy)^{-}(dpp\text{-}bian)^{2-}\cdot Mg(DME)]$ **3a**. Its barium analogue, compound $[(dpp\text{-}bian)^{2-}Ba(DME)_2(4,4'\text{-}bipy)^0(dpp\text{-}bian)^{2-}Ba(DME)_2]$ **3b**, has been prepared by reacting of $[(dpp\text{-}bian)Ba(THF)_n]$ with 0.5 molar equiv. of 4,4′-bipy. Although complexes **3a**,**b** consist of the same redox-active ligands, they differ in electronic structure and represent virtual redox-isomers. The investigation of the redox-behavior of complexes 1D coordination polymers of group 2 metals is in progress and will be published elsewhere.

This study was supported by the Russian Science Foundation (grant no. 19-13-00336). The work was performed using the equipment of 'Analytical Center of the IOMC RAS' in G. A. Razuvaev Institute of Organometallic Chemistry RAS within the Project 'Ensuring of development of material and technical infrastructure of the centers for collective use of scientific equipment' (identification no. RF-2296.61321X0017, agreement no. 075-15-2021-670). V.I.O. and A.S.B. thank the Russian Science Foundation (grant no. 18-13-00380, magnetochemistry).

Online Supplementary Materials

Supplementary data associated with this article can be found in the online version at doi: 10.1016/j.mencom.2022.11.017.

References

1 *The Chemistry of Metal-Organic Frameworks: Synthesis, Characterization, and Applications*, ed. S. Kaskel, Wiley-VCH, Weinheim, 2016.
2 H. Furukawa, K. E. Cordova, M. O'Keeffe and O. M. Yaghi, *Science*, 2013, **341**, 974.
3 A. U. Czaja, N. Trukhan and U. Müller, *Chem. Soc. Rev*., 2009, **38**, 1284.
4 A. Yu. Tsivadze, O. E. Aksyutin, A. G. Ishkov, M. K. Knyazeva, O. V. Solovtsova, I. E. Men'shchikov, A. A. Fomkin, A. V. Shkolin, E. V. Khozina and V. A. Grachev, *Russ. Chem. Rev.*, 2019, **88**, 925.
5 Y. M. Litvinova, Y. M. Gayfulin, K. A. Kovalenko, D. G. Samsonenko, J. van Leusen, I. V. Korolkov, V. P. Fedin and Y. V. Mironov, *Inorg. Chem*., 2018, **57**, 2072.
6 M. Bláha, V. Valeš, Z. Bastl, M. Kalbáč and H. Shiozawa, *J. Phys. Chem*., 2020, **124**, 24245.
7 H.-Y. Wang, L. Cui, J.-Z. Xie, C. F. Leong, D. M. D'Alessandro and J.-L. Zuo, *Coord. Chem. Rev.*, 2017, **345**, 342.
8 X. Zhang, I. da Silva, R. Fazzi, A. M. Sheveleva, X. Han, B. F. Spencer, S. A. Sapchenko, F. Tuna, E. J. L. McInnes, M. Li, S. Yang and M. Schröder, *Inorg. Chem*., 2019, **58**, 14145.
9 X. Han, W. Lu, Y. Chen, I. da Silva, J. Li, L. Lin, W. Li, A. M. Sheveleva, H. G. W. Godfrey, Z. Lu, F. Tuna, E. J. L. McInnes, Y. Cheng, L. L. Daemen, L. J. McCormick McPherson, S. J. Teat, M. D. Frogley, S. Rudić, P. Manuel, A. J. Ramirez-Cuesta, S. Yang and M. Schröder, *J. Am. Chem. Soc*., 2021, **143**, 3153.
10 P. Cai, W. Chen, G. S. Day, H. F. Drake, E. A. Joseph, Z. T. Perry, Z. Xiao and H.-C. Zhou, in *Comprehensive Nanoscience and Nanotechnology*, eds. D. L. Andrews, R. H. Lipson and T. Nann, Elsevier, Amsterdam, 2019, pp. 35–54.
11 F. Bigdeli, C. T. Lollar, A. Morsali and H.-C. Zhou, *Angew. Chem., Int. Ed*., 2020, **59**, 4652.
12 J. Calbo, M. J. Golomb and A. Walsh, *J. Mater. Chem. A*, 2019, **7**, 16571.
13 J. Su, S. Yuan, J. Li, H.-Y. Wang, J.-Y. Ge, H. F. Drake, Yu, F. Leong, D. M. D'Alessandro, M. Kurmoo, J.-L. Zuo and H.-C. Zhou, *Chem. – Eur. J*., 2021, **27**, 622.
14 B. Li, Y.-M. Zhao, A. Kirchon, J.-D. Pang, X.-Y. Yang, G.-L. Zhuang and H.-C. Zhou, *J. Am. Chem. Soc*., 2019, **141**, 6822.
15 M. I. Rogovoy, A. V. Tomilenko, D. G. Samsonenko, N. A. Nedolya, M. I. Rakhmanova and A. V. Artem'ev, *Mendeleev Commun.*, 2020, **30**, 728.
16 B. Ding, M. B. Solomon, C. F. Leong and D. M. D'Alessandro, *Coord. Chem. Rev.*, 2021, **439**, 213891.
17 N. L. Bazyakina, V. M. Makarov, S. Yu. Ketkov, A. S. Bogomyakov, R. V. Rumyantcev, V. I. Ovcharenko and I. L. Fedushkin, *Inorg. Chem*., 2021, **60**, 3238.
18 R. Zhang, Y. Wang, Y. Zhao, C. Redshaw, I. L. Fedushkin, B. Wu and X.-J. Yang, *Dalton Trans*., 2021, **50**, 13634.
19 I. L. Fedushkin, A. S. Nikipelov, A. A. Skatova, O. V. Maslova, A. N. Lukoyanov, G. K. Fukin and A. V. Cherkasov, *Eur. J. Inorg. Chem*., 2009, 3742.
20 A. G. Morozov, M. V. Moskalev, D. A. Razborov and I. L. Fedushkin, *J. Organomet. Chem.*, 2020, **927**, 121535.
21 I. L. Fedushkin, A. A. Skatova, V. A. Chudakova, G. K. Fukin, S. Dechert and H. Schumann, *Eur. J. Inorg. Chem.*, 2003, 3336.
22 M. S. Denning, M. Irwin and J. M. Goicoechea, *Inorg. Chem*., 2008, **47**, 6118.
23 I. L. Fedushkin, A. G. Morozov, O. V. Rassadin and G. K. Fukin, *Chem. – Eur. J*., 2005, **11**, 5749.
24 M. Irwin, T. Krämer, J. E. McGrady and J. M. Goicoechea, *Inorg. Chem*., 2011, **50**, 5006.
25 S. Stoll and A. J. Schweiger, *J. Magn. Reson*., 2006, **178**, 42.
26 C. B. Benda and T. F. Fässler, *Z. Naturforsch*., 2014, **69b**, 1119.
27 N. L. Bazyakina, M. V. Moskalev, A. V. Cherkasov, V. M. Makarov and I. L. Fedushkin, *CrystEngComm*, 2022, **24**, 2297.
28 *SAINT, Data Reduction and Correction Program, Version 8.38A*, Bruker AXS, Madison, WI, 2017.
29 L. Krause, R. Herbst-Irmer, G. M. Sheldrick and D. Stalke, *J. Appl. Crystallogr.*, 2015, **48**, 3.
30 G. M. Sheldrick, *Acta Crystallogr., Sect. A.: Found. Adv.*, 2015, **71**, 3.
31 G. M. Sheldrick, *Acta Crystallogr., Sect. C: Struct. Chem*., 2015, **71**, 3.
32 G. M. Sheldrick, *SHELXTL, Version 6.14, Structure Determination Software Suite*, Bruker AXS, Madison, WI, 2003.
33 A. L. Spek, *Acta Crystallogr., Sect. C: Struct. Chem.*, 2015, **71**, 9.

Received: 27th May 2022; Com. 22/6916